



HAL
open science

Hydraulic visibility: Using satellite altimetry to parameterize a hydraulic model of an ungauged reach of a braided river

Pierre-André Garambois, Stéphane Calmant, Hélène Roux, Adrien Paris, Jerome Monnier, Pascal Finaud-Guyot, Amanda Samine Montazem, Joecila Santos da Silva

► To cite this version:

Pierre-André Garambois, Stéphane Calmant, Hélène Roux, Adrien Paris, Jerome Monnier, et al.. Hydraulic visibility: Using satellite altimetry to parameterize a hydraulic model of an ungauged reach of a braided river. *Hydrological Processes*, 2017, 31 (4), pp.756-767. 10.1002/hyp.11033 . hal-01711044

HAL Id: hal-01711044

<https://hal.science/hal-01711044>

Submitted on 16 Feb 2018

HAL is a multi-disciplinary open access archive for the deposit and dissemination of scientific research documents, whether they are published or not. The documents may come from teaching and research institutions in France or abroad, or from public or private research centers.

L'archive ouverte pluridisciplinaire **HAL**, est destinée au dépôt et à la diffusion de documents scientifiques de niveau recherche, publiés ou non, émanant des établissements d'enseignement et de recherche français ou étrangers, des laboratoires publics ou privés.




Open Archive TOULOUSE Archive Ouverte (OATAO)

OATAO is an open access repository that collects the work of Toulouse researchers and makes it freely available over the web where possible.


This is an author-deposited version published in : <http://oatao.univ-toulouse.fr/>
Eprints ID : 19570

To link to this article : DOI:10.1002/hyp.11033
URL : <http://dx.doi.org/10.1002/hyp.11033>

To cite this version : Garambois, Pierre-André and Calmant, Stéphane and Roux, Hélène  and Paris, Adrien and Monnier, Jérôme and Finaud-Guyot, Pascal and Montazem, Amanda Samine and Santos da Silva, Joecila *Hydraulic visibility: Using satellite altimetry to parameterize a hydraulic model of an ungauged reach of a braided river*. (2017) *Hydrological Processes*, vol. 31 (n° 4). pp. 756-767. ISSN 0885-6087

Any correspondence concerning this service should be sent to the repository administrator: staff-oatao@listes-diff.inp-toulouse.fr

Hydraulic visibility: Using satellite altimetry to parameterize a hydraulic model of an ungauged reach of a braided river

Pierre-André Garambois¹ | Stéphane Calmant² | Hélène Roux³ |
Adrien Paris²  | Jérôme Monnier⁴ | Pascal Finaud-Guyot⁶ |
Amanda Samine Montazem² | Joecila Santos da Silva⁵

¹ICUBE - UMR 7357, Fluid Mechanics Team, INSA Strasbourg, 24 Boulevard de la victoire Strasbourg cedex, 67084, France

²Université Toulouse III Paul Sabatier, OMP, Laboratoire D'Etudes EN Géophysique et Océanographie Spatiales (UMR 5566 CNES CNRS IRD UPS), Toulouse, France

³Université de Toulouse, INPT, UPS, IMFT (Institut de Mécanique des Fluides de Toulouse), CNRS, Allée Camille Soula, Toulouse, 31400, France

⁴Mathematics Institute of Toulouse - National Institute for Applied Sciences, 135 Avenue de Rangueil Toulouse Cedex 4, 31077, France

⁵CESTU/UEA, Manaus, Brazil

⁶ICUBE - UMR 7357, Fluid Mechanics Team, Strasbourg Cedex, 67000, France

Correspondence

Pierre-André Garambois, ICUBE - UMR 7357, Fluid Mechanics Team, INSA Strasbourg, 24 Boulevard de la victoire, 67084 Strasbourg cedex, France.

Email: pierre-andre.garambois@insa-strasbourg.fr

Funding Information

CNES, TOSCA.

Abstract

What hydraulic information can be gained from remotely sensed observations of a river's surface? In this study, we analyze the relationship between river bed undulations and water surfaces for an ungauged reach of the Xingu River, a first-order tributary of the Amazon river. This braided reach is crosscut more than 10 times by a ENVISAT (ENVironmental SATellite) track that extends over 100 km. Rating curves based on a modeled discharge series and altimetric measurements are used, including the zero-flow depth Z_0 parameter, which describes river's bathymetry. River widths are determined from JERS (Japanese Earth Ressources Satellite) images. Hydrodynamic laws predict that irregularities in the geometry of a river bed produce spatial and temporal variations in the water level, as well as in its slope. Observation of these changes is a goal of the Surface Water and Ocean Topography satellite mission, which has a final objective of determining river discharge. First, the concept of hydraulic visibility is introduced, and the seasonality of water surface slope is highlighted along with different flow regimes and reach behaviors. Then, we propose a new single-thread effective hydraulic approach for modeling braided rivers flows, based on the observation scales of current satellite altimetry. The effective hydraulic model is able to reproduce water surface elevations derived by satellite altimetry, and it shows that hydrodynamical signatures are more visible in areas where the river bed morphology varies significantly and for reaches with strong downstream control. The results of this study suggest that longitudinal variations of the slope might be an interesting criteria for the analysis of river segmentation into elementary reaches for the Surface Water Ocean Topography mission that will provide continuous measurements of the water surface elevations, the slopes, and the reach widths.

KEYWORDS

braided rivers, effective hydraulics, hydrodynamical signature, satellite altimetry

1 | CONTEXT OF THE ISSUE

Although the discharge of streams and rivers is an important component of the water cycle and represents a vital issue for societies worldwide, the runoff of the largest global basins is still poorly monitored, and the number of gauges and access to these data are decreasing across the world (Bjerklie, Moller, Smith, & Dingman, 2005; Vörösmarty et al., 2010). New generations of satellite and sensors offer the potential to overcome this lack of in situ data for hydrological sciences (Calmant et al., 2008; Alsdorf & Lettenmaier, 2003).

Satellite measurements have led to interesting results for continental hydrosystems, including surface water monitoring via altimetry throughout global watersheds (Koblinsky, Clarke, Brenne, & Frey, 1993;

Morris & Gill, 1994; Smith, Isacks, Bloom, & Murray, 1996; Smith, 1997; Birkett, 1998; Mercier, Cazenave, & Maheu, 2002; Maheu, Cazenave, & Mechoso, 2003; Kouraev, Zakharova, Samain, Mognard, & Cazenave, 2004; Berry, Garlick, Freeman, & Mathers 2005; Calmant & Seyler, 2006; Crétaux and Birkett, 2006; Frappart, Calmant, Cauhopé, Seyler, & Cazenave, 2006; Zakharova, Kouraev, Cazenave, & Seyler, 2006; Alsdorf, Rodríguez, and Lettenmaier, 2007b; Roux et al., 2008; Birkinshaw et al., 2010; Papa et al., 2010; Roux et al., 2010; Lee et al., 2011; Santos da Silva et al., 2012), large flood extent estimation based on synthetic aperture radar (e.g., Hess, Melack, Filoso, & Wang, 1995; Bates et al., 2006; Alsdorf, Bates, Melack, Wilson, & Dunne 2007a; Schumann et al., 2007; Kim et al., 2009; Hostache, Lai, Monnier, & Puech, 2010), optical imagery (Pandey et al., 2014) or microwave sensors imagery

(Papa et al., 2008; Prigent et al., 2012), large-scale change in water mass distribution (Lettenmaier & Famiglietti, 2006; Ramillien, Cazenave, & Brunau, 2004; Ramillien, Famiglietti, & Wahr 2008; Smith et al., 2009; Chen, Wilson, & Tapley 2010; Xavier et al., 2010; Frappart, Seoane, & Ramillien, 2013a; Frappart, Ramillien, & Ronchail, 2013b; Ramillien, Frappart, & Seoane, 2014), water quality (Koponen et al., 2004), and solid discharge data (Martinez, Guyot, Filizola, & Sondag, 2009) or even groundwater tables data (Meijerink, 1996; Pfeffer et al., 2014). Several statistical methods for estimating river discharge associating space-borne data and ground-based ancillary data have been proposed (Bjerklie et al., 2005; Leon et al., 2006; Papa et al., 2010; Getirana & Peters-Lidard, 2012; Tarpanelli et al., 2013; Birkinshaw et al., 2014 among others). The forthcoming Surface Water and Ocean Topography (SWOT) mission, which is dedicated to the observation of global water storage and fluxes, will provide water surface measurements of continental water bodies at a decimetric vertical accuracy over river areas of 1 km² and rivers wider than 100m. Studies have recently proposed primary methods for estimating river discharge from SWOT data, such as datasets consisting of water river surface elevation, widths and slopes (Durand et al., 2014; Garambois & Monnier, 2015; Gleason & Smith, 2014; Gleason, Smith, & Lee, 2014), as well as an intercomparison (Yoon et al. 2016; Durand et al. Moderate revisions). However, when retrieving discharge values from open channel flow equations that are constrained by the sole water surface elevation (WSE) observations, the difficulty of measuring the bathymetry and roughness of the river channels from spaceborne or airborne satellites must be considered.

In this context, Garambois and Monnier (2015) demonstrated that for a specific observation scale, an adequate inverse modeling scale and physical complexity exist for river flows in single-thread natural channels. However, a considerable number of global rivers present a more complex morphology such as braided rivers. O'Loughlin, Trigg, Schumann, and Bates (2013) studied approximately 1,600 km of the middle Congo reach, which is mostly braided, evaluated the possible hydraulic control sections based on water surface width observations using Landsat imagery and associated these observations with water surface slope and backwater effects. The authors produced water surface slope profiles based on Ice, Cloud, and land Elevation Satellite WSEs and found that they were nearly constant over time for the period corresponding to the falling limb (March), low water (June), and the rising limb (November). However, these water surface slope profiles are calculated based on unevenly spatiotemporal data, which included 256 time points/locations for the 1,600-km reach. The minimum spatial gap was approximately 25 km, and the mean spatial gap was graphically estimated as approximately 50 km or more, which prevents a deeper flow behavior analysis and might have caused a lack of hydraulic visibility in terms of water surface curvature as shown in the present paper, which includes a rather dense spatiotemporal sampling of a 80-km reach of the Xingu River. Moreover, the control sections in the present paper are analyzed with regard to cross-sectional and longitudinal variations of river bed elevation and cross-sectional shapes as predicted by the hydrodynamic equations.

Most studies that have incorporated remotely sensed WSEs, generally for distant river reaches, are performed for river with several available bathymetry measurements. Water elevations can then be assimilated into a hydraulic model with known bathymetry, such as in models designed (e.g., Hostache et al., 2010; Biancamaria et al.,

2011). Siddique-E-Akbor, Hossain, Lee, and Shum (2011) examined the consistency in the water elevations data for the main rivers of the Bangladesh delta between satellite altimetry data and a 1D calibrated hydraulic model. Even with a hydraulic model calibrated on in situ water depth gauges, the authors observed an average root-mean-square error of 2 m between ENVISAT data and the modeled WSEs for this complex deltaic environment. Different altitude references between altimetry and in situ data could explain a portion of this error budget. To the best of our knowledge, this study introduces one of the first hydraulic modeling of an ungauged river reach based on altimetric data. This work proposes a new effective hydraulic approach for modeling braided river sections, based on the observation scales of current satellite altimetry and in view of the future SWOT mission.

For a given hydrologic signal, hydrodynamic laws predict that longitudinal variations in a river bed's elevation and cross-sectional shape will produce spatial variations in the water level and thus in the slope of the water line. Recently, Paris et al. (2016) proposed a set of river bed elevations of the Amazon basin based on a large altimetric dataset first published in Santos da Silva et al. (2012) as well as discharge from the continuous distributed rainfall runoff model MGB-IPH published in Paiva et al. (2013).

Using rating curve parameters calibrated by Paris et al. (2016) (cf., Section 2.2), the objectives of the present paper are twofold:

- Investigate the hydraulic meaning of state-of-the-art altimetric WSE measurements.
- Test whether a real braided river with seasonal overbanking dynamics can be modeled using a single-thread effective representation and calibrated roughness.

We use a hydrodynamic model (cf., Sections 3.1 and 3.2) to investigate the consistency of river bed undulations derived from stage-discharge rating curves and the spatial and temporal variability of water surface slopes derived from ENVISAT satellite altimetry for a braided reach of the Xingu river, which is a first-order tributary of the Amazon River. This river is crosscut more than 10 times by a single ENVISAT track that extends over a hundred kilometers, thereby providing direct access to instantaneous WSE and slopes approximations (downstream finite difference) and their temporal variations and indirect access to a longitudinal river bed elevation for this reach of the Xingu River based on the method of Paris et al., (2016). The water surface width of the reaches and their variations with the hydrological cycle cannot be inferred using current altimetry products. Therefore, the reach widths are obtained from SAR (Synthetic Aperture Radar) imagery mosaics derived from the JERS mission of the Global Rain Forest Mapping project. A simple and effective representation of braided river sections/reaches based on real "state-of-the-art data" is proposed.

High-resolution observations of the variations in elevation and slope of the WSE worldwide is a goal of the future-wide swath altimetric mission SWOT, which will be launched in 2021 by National Aeronautics and Space Administration and CNES (Centre National d'Études Spatiales), which has a final goal of determining river's discharges (see Biancamaria et al., 2010; Biancamaria, 2016). This study aims to constitute a low-resolution baseline for hydraulic analyzes and inverse methods that use higher resolution data such as those expected from SWOT.

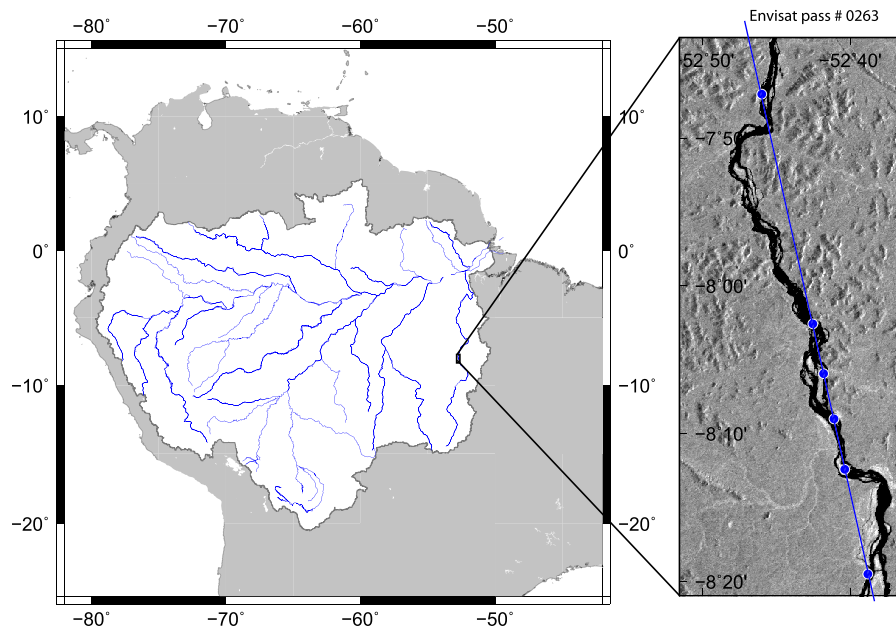


FIGURE 1 Study site: Xingu River reach within the Amazon watershed, virtual stations SV#12 to SV#1 from south to north

The paper is structured as follows. Section 2 introduces the study zone and data and provides an analysis of water surface slope variability. Section 3 describes the hydrodynamic model and hypotheses. And Sections 4 and 5 present results and discussions.

2 | UNGAUGED BRAIDED RIVER REACH WITH LONG ALTIMETRIC RECORDS

2.1 | Study zone

From its headwaters in the Andes mountains to its delta at Atlantic Ocean, the Amazon drains an area of approximately 6.1×10^6 km² and has an average discharge on the order of 2.10^5 m³.s⁻¹ (e.g., Richey et al., 1989). The Xingu River, which has a drainage area of approximately 5.3×10^5 km² and an average discharge on the order of 9.10^3 m³.s⁻¹, is a first-order southeast tributary at its confluence with the Amazon. The study zone consists of an ungauged braided reach of the Xingu River where six virtual stations (VS) have been defined according to ENVISAT measurements (Figure 1). This reach was selected for the following reasons:

- It is an ungauged reach; thus, it represents a challenging point for hydrological and hydraulics research;
- It is crosscut more than 10 times by a single ENVISAT track, which is quite rare;
- Several important contributions are available for the Amazon basin where the reach of the Xingu River is located: calibrated hydrological model MGB (Paiva et al., 2013), altimetric dataset (Santos da Silva et al., 2012), and fairly accurate altimetric rating curves (Paris et al., 2016).

As highlighted by Santos da Silva et al. (2012), ENVISAT altimetric data are convenient for the study of continental water bodies that

present vertical errors and are typically located between 0.12 and 0.4 m in the Amazon basin. The six virtual stations derived from the ENVISAT dataset in the study area define five reaches for a total length of 72 km along the Xingu River (Table 1). A significant tributary is not observed for this river section. The series encompass the entire ENVISAT mission from mid-2002 to mid-2010 with WSE measurements at each VS every 35 days, thereby representing 76 samples of WSE. In-depth descriptions on the processing of the raw ENVISAT data are provided in Santos da Silva et al. (2012). Cross-sectional water surface width were obtained from tow JERS mosaics¹: one for the low water period, which uses the images collected between September and December 1995, and one for the high water period, which uses images collected between May and August 1996. In these mosaics, the river channels are characterized by a very low radar echo returns, because of inundated forest on the margins of the river channel are characterized by very high returns due to the double bounce effect on the radar pulse. The magnitude of the retro-diffusion is scaled between 0 and 255 in the products. Based on the work conducted by Hess, Melack, Novo, Barbosa, and Gastil, (2003), who classified the retro-diffusion coefficients of the JERS-1 images in the Amazon basin, we used a threshold value of ≤ 50 to identify the minor bed of the rivers at the low water season and a threshold value of at least 180 at least to characterize the forest flooded at the high water season. These values were used to estimate the major bed of the river at the high water season. For the braided sections, the width included in the effective model hereafter is determined according to the sum of each thread's width. A JERS image at low water season in the study area is shown in the right panel of Figure 1. The effective water surface widths corresponding to the total top width of all threads are represented for low and high flows in Figure 2

¹Courtesy of GRFM, (c) NASDA/MITI

TABLE 1 Rating curve parameters a , b , and bathymetry Z_0 are from Paris et al. (2016) for the six virtual stations selected in this study along 72 km of the Xingu River

	VS#12	VS#11	VS#6	VS#5	VS#3	VS#1
Distance to mouth [km]	1,146	1,129	1,124	1,116	1,110	1,075
Drainage area [km ²] (MGB model)	193,255	193,255	194,148	194,148	195,882	197,862
Z_0 [m] (reference: EGM2008)	209.6	207.1	206.9	206.5	204.3	196.5
a	162.514	74.631	74.72	143.708	59.184	103.925
b	2.204	2.543	2.633	2.52	2.715	2.288
Total low flow width [m] (derived from JERS)	1,090	1,540	1,260	1,590	930	930
Total high flow width [m] (derived from JERS)	2,610	1,850	1,900	2,240	1,240	1,140

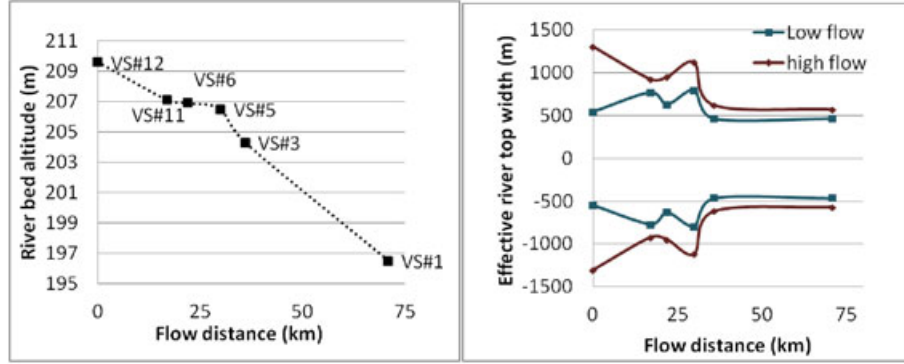


FIGURE 2 Representation of (left) the river bed bathymetry Z_0 from Paris et al. (2016) and (right) the effective water surface top width derived from JERS images between the left and right banks

2.2 | Altimetry-based rating curves and river bed elevations

This section briefly introduces the stage–discharge relationships among the river reaches and river bed elevations proposed by Paris et al. (2016) for the Amazon basin. Those rating curves are based on altimetric database from the ENVISAT and JASON-2 altimetric missions for the WSEs at 920 VS throughout the Amazon basin proposed by Santos da Silva et al. (2012) and discharge data calculated by Paiva et al. (2013) using the distributed rainfall-runoff model MGB. To interpret the rating curve parameters in terms of the hydrological and morphological parameters of river reaches, the stage $Z(t)$ and discharge $Q(t)$ series were fitted by Manning-like power laws. The Manning equation for large rivers writes:

$$Q(t) = K w h^{5/3} S^{1/2}, \quad (1)$$

where h is the water depth, w is the width of the rectangular cross section, K is the Strickler friction coefficient, and S is the slope of the water line. The rating curve general expression used by Paris et al. (2016) for a given river cross section abscissa x is as follows:

$$Q(x, t) = a(x) [Z(x, t) - Z_0(x)]^{b(x)}, \quad (2)$$

where a , b , and Z_0 are the rating curve parameters optimized with an algorithm based on a Markov chain Monte Carlo method in a Bayesian framework (the Shuffled Complex Evolution Metropolis-UA) by Vrugt, Gupta, Bastidas, Bouten, and Sorooshian (2003) with a cost function based on the difference between calculated and MGB discharges. Assuming the equivalence with the Manning Equation 1, the likely rating curve parameters from Equation 2 are $a = WK S^{1/2}$, and Z_0 that is the river bed elevation that references the same geodetic system

as the altimetric series. Paris et al. (2016) showed that the rating curve parameters for which the coefficients were optimized over 8 years of ENVISAT and Jason-2 measurements were consistent with the in situ ADCP (Acoustic Doppler Current Profiler) measurements, and especially the mean river bed elevation Z_0 , which had an error of about 5% compared with the area-to-width ratio of the ADCP cross sections. Additionally, these rating curves are not mission specific, and the rated discharge can be estimated with WSE data gained from in situ measurements or altimetric missions.

3 | EFFECTIVE MODEL OF A BRAIDED RIVER REACH

In this section, an effective model \mathcal{M}_{eff} with averaged hydraulic parameters is defined. Indeed, the definition of river reach boundaries with average hydraulic properties is somehow imposed by the spatial scale of the WSE observations from the satellite. Note that the definition of a river reach is an important step for forward hydraulic modeling but also for inverse methods, such as for discharge retrieval (e.g., Garambois & Monnier, 2015; Durand et al., 2014) via conditioning inverse problem complexity. One goal of the current contribution is to investigate a simple and effective representation of braided river section/reaches so that flow dynamics can be analyzed for a relatively coarse bathymetry derived from altimetric rating curves (Paris et al., 2016).

3.1 | Cross-sectional representation

As shown in Figure 1, the five reaches studied in this paper are braided. Because detailed data on the exact bathymetry of the reaches and

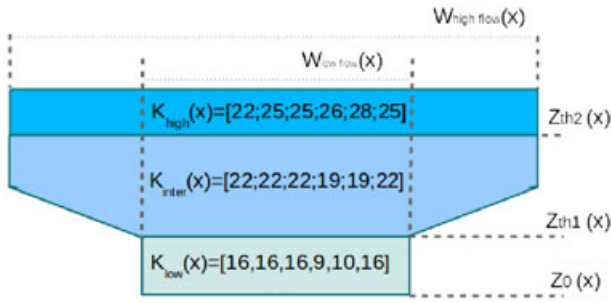


FIGURE 3 Hypothesis of the effective model \mathcal{M}_{eff} (geometry, calibrated river roughness distribution K_s between brackets for the three defined flow regimes) for the forward backwater curve resolutions. Threshold defined for the downstream cross section VS#1, $Z_{th1} = 198.82$ m and $Z_{th2} = 201.77$ m

measurements of different WSE in the small channels contouring the islets are not available, we used an effective representation of the real braided morphology that consists of a single channel with a parameterization that results in an equivalent hydrodynamical behavior. The goal is to model the WSE and slopes that are likely consistent with those measured by satellite altimetry. The hypothesis of a single thread is required by the spatial resolution of the current altimetry measurements so that flow parameters can be identified. The shape of the cross sections is defined according to the observational capabilities and limitations: For values below the lower flow observation, each section is assumed to be rectangular with the Z_0 parameter (river bed elevations) taken from Paris et al. (2016), whereas for values above this observation, a trapezoidal approximation of the cross section within the bounds given by the JERS imagery is affordable (cf, Garambois & Monnier, 2015; Durand et al., 2014). However, a variable spatiotemporal roughness coefficient is required in this study, and it is discussed in Sections 4 and 5. Based on the cross section definition and to ensure that the roughness hence the discharge will be a continuous function of the water elevation Z , let us define the Strickler coefficient $K(Z)$ for each virtual station as follows:

$$K_s(Z) = \begin{cases} K_{low} & Z < Z_{th1} \\ K_{low} + (K_{inter} - K_{low}) \tanh(Z - Z_{th1}) & \text{if } Z_{th1} < Z < Z_{th2} \\ K_{inter} + (K_{high} - K_{inter}) \tanh(Z - Z_{th2}) & Z_{th2} < Z. \end{cases} \quad (3)$$

with Z_{th1} and Z_{th2} representing respectively the thresholds of the water elevation for low-intermediate and intermediate-high flows, respectively, as defined for the downstream cross section VS#1 (Figure 3). Therefore, the following three flow regimes are defined: low, medium, and high flow (Equation 3). When a threshold is reached for VS#1 WSE, we consider that this threshold also applies to each upstream cross sections (resolution from downstream to upstream cf., Section 3.2,). The roughness calibration is detailed in Section 4.3.

3.2 | Gradually varied steady-state flows

The time scale of observations—monthly—does not allow to observe fast temporal dynamics; thus, we assume permanent states of the river reaches at each observation time. For permanent flows, the

Saint-Venant equations reduce to the backwater curve equation:

$$\partial_x Q = 0. \quad (4)$$

$$\partial_x h = \frac{I - J}{1 - Fr^2}. \quad (5)$$

where $Q[\text{m}^3 \cdot \text{s}^{-1}]$ is the cross-sectional discharge, $h[\text{m}]$ is the water depth determined from the river bed averaged across the channel, $I = -\partial_x Z_0$ is the river bed slope $[\text{m} \cdot \text{m}^{-1}]$, and $J = \frac{Q|Q|}{K_s^2 A^2 R_h^{\frac{4}{3}}}$ is the energy slope $[\text{m} \cdot \text{m}^{-1}]$ calculated with Manning-Strickler formula. K is the Strickler roughness coefficient $[\text{m}^{\frac{1}{3}} \cdot \text{s}^{-1}]$, A is the cross-sectional wetted area $[\text{m}^2]$, and R_h is the hydraulic radius defined as the ratio between wetted the wetted surface and perimeter, Fr is the Froude number such as $Fr^2 = \frac{Q^2 w}{g A^3}$, where w is the water surface width $[\text{m}]$ and g is the gravity acceleration of the Earth $[\text{m} \cdot \text{s}^{-2}]$. The water depth h is related to the WSE Z measured by altimetry: $h = Z - Z_0$. Note that because Z_0 is obtained by the rating curves from Paris et al. (2016), which is based on the altimetry data, Z and Z_0 are directly referenced to the same datum, which is the EGM2008 global geoid model in our case.

The systems of Equations 4 and 5 are first-order differential equations in x ; therefore, one boundary condition is necessary for each variable Q and h . When the flow is sub-critical ($Fr^2 < 1$), a downstream boundary condition is required, that is, at the outlet of the domain. We used a high-order Runge-Kutta numerical scheme to accurately solve these systems of differential equations.

4 | RESULTS

4.1 | Water surface variability observed by altimetry

The analysis of the WSEs and slopes, from 76 ENVISAT overpasses selected between 2002 and 2010, is presented in Figure 4. The hydrograms presented in Figure 4 demonstrate the alternation between wet and dry seasons of an average hydrological year, with one clear annual flood peak in March and low waters in September (Figure 4a). Such a regime is typical for large river systems located in tropical areas (cf, Birkett, 1998). The elevation difference between the lowest and the highest WSE varies from 4 m for VS#5 to 5.7 m for VS#1, as shown by the blue envelope in Figure 4b. These variations are consistent with the 4.4-m variation depicted by the stage series at Sao-Miguel X5, which is the closest gauge to the study area (located ~200 km downstream) and has the same months of high and low flows (<http://hidroweb.ana.gov.br>). Such a difference in water level dynamics between the VS#5 and VS#1, which are only separated by approximately 40 km and do not present water inflow from a tributary, must be attributed to a significant change in river morphology such as in the cross-sectional area and/or in the bed slope.

The water surface slopes, which were calculated from the WSEs at two virtual stations divided by the flow distance, range between 3 and 35 cm/km. The water surface slopes of the last two reaches of the studied domain were the highest (Figure 4d). More importantly, the monthly averages of the slopes highlighted a seasonality in water surface slope variability for the reaches as plotted in Figure 4c. The water surface slopes are less undulated over the whole studied domain for higher flow conditions (cf, Figure 4c,d). For example, in March, the slope difference between the steepest and the flattest reach is about 12 cm/km,

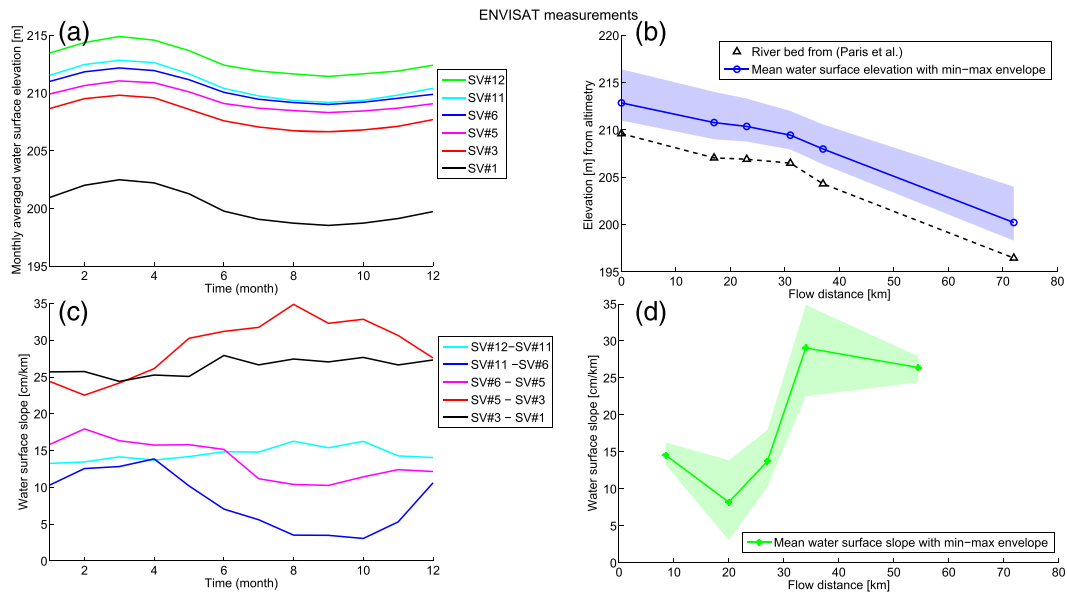


FIGURE 4 Analysis of ENVISAT data: (a) monthly average for water surface elevation at each virtual stations (VS); (b) mean, minimum, and maximum (blue envelope) water surface elevation with river bed elevation Z_0 according to Paris et al. (2016); (c) monthly average for the water surface slope for each reach between two VS; and (d) mean, minimum and maximum (green envelope) water surface slope

whereas in August, this slope difference is about 30 cm/km. In other words, the spatial variability of the river morphology is more filtered by the water surface profile for higher flow conditions (in March), which can be depicted here according to altimetric measurements of the WSE.

4.2 | Hydraulic characterization of reach behavior using 8 years of altimetric records

Free surface flow dynamics are controlled by boundary conditions (inlet(s), outlet(s), and basal friction) and the river morphology, that is, longitudinal variations of the river bed slope and/or cross-sectional area. For reaches between VS#11 and VS#6 and VS#6 and VS#5, water surface slopes tend to decrease when water level decreases and vice versa (Figure 4c). A decrease in the water surface slope for lower flows may indicate stronger downstream control. On the contrary, for the reach between VS#5 and VS#3, the water surface slope tends to increase when the water level decreases. Hence, the flow behavior may change between the lowest and the highest flow regime, from an unsubmerged to submerged weir flow behavior for those three reaches. No particular trend can be depicted from the variations in water surface slope for the other longer reaches between VS#12 and VS#11 and VS#3 and VS#1. The most downstream reach, which is between VS#11 and VS#12, is the longest reach of this study. This lack of visible variability may have been caused by spatial resolution that was too coarse for such long reaches. As shown in Section 4.4, the spatial resolution of the altimetric dataset and the hydraulic model used in this paper allows us to depict water surface variability along the study domain and within contrasted flow regimes. Using analogous terminology for meteorological radars and hydrologic visibility of rainfall fields (Pellarin et al., 2002), we define hydraulic visibility, the potential to depict a hydrological response, and hydraulic variabilities within a river section or network via remote sensing.

The flow behavior and downstream control effects are significantly linked to a channel's geometry. The river bed slope breaks around near VS#5, and the river cross-sectional area and shape variability may have an influence on flow dynamics. The effective river top width in Figure 2 for a low river effective width varies slightly at approximately 1,000 m with a +30% variation for VS#11 and VS#5. For high flows, a sharp effective width constriction appears from upstream to downstream in the studied domain, and rapid constrictions of river top widths have also been reported by O'Loughlin et al. (2013) for the Congo River. For the Xingu, the effective high-flow top-width varies from 2,240 to 1,240 m at a 6-km flow distance between VS# 5 and VS#3.

4.3 | Calibration/validation of the effective hydraulic model

A permanent flow line is simulated for each satellite pass by solving the backwater curve Equation 5. For each reach, we use the discharge calculated from the altimetric rating curves. The WSE measured by ENVISAT at VS#1 downstream of the studied domain is used as boundary condition for the water depth (because the estimated bathymetry parameter elevation Z_0 is available). The roughness distribution along the river reach is calibrated through a trial and error procedure designed to minimizing the distance between the simulated (Equation 5) and observed flow lines on the calibration period formed by the first 38 ENVISAT passes.

The accuracy of the modeled flow lines is first analyzed in terms of the relative elevation error with respect to the WSE measured by ENVISAT at the five remaining upstream virtual stations (Figure 5). In the left panel of Figure 5, the calibration results are fairly good and present a median error lower than 3.5% and an interquartile range on the order or lower than 10%. Comparable results are obtained for the validation on the remaining 38 passes, which presents few more absolute error values ranging between 10% and 15%. Moreover, reasonable

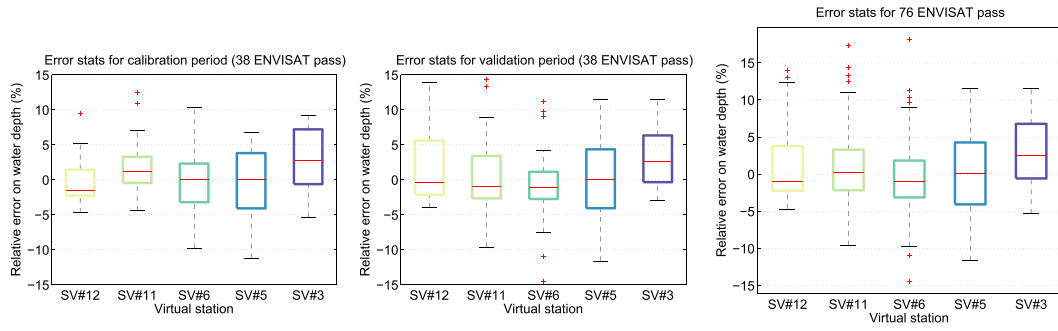


FIGURE 5 Relative error $Err = \frac{(Z - Z_{alt})}{(Z_{alt} - Z_0)}$ between the modeled WSE and ENVISAT data for simulated water depths with effective cross sections determined using calibration (left) and validation (middle) subsets and the whole dataset (right), that is, 76 satellite overpass between 13/11/2002 and 22/09/2010, $mean_t(Err) = 0.038$, $Q_{50} = 0.024$

roughness values ranging from 9 to 28 (i.e., Manning coefficient ranging from 0.036 to 0.11) were found (Figure 5) compared with the usual ranges (e.g., Chow, 1959).

4.4 | Retrieving flow line dynamics and rating curves

Flow lines simulated with the above method are presented in Figure 6. Various flow regimes can be reproduced via the representation of the cross sections and the parameterization of the calibrated roughness varying with the WSE. As shown in the right panel of Figure 6, the consistency between the simulated WSE and the measurements for the 76 satellite overpasses is fairly good. For flow conditions ranging from $423 \text{ m}^3/\text{s}$ to $10,574 \text{ m}^3/\text{s}$, the mean and median relative error on the WSE are 3.8% and 2.4%.

We show three modeled flow lines that correspond to the contrasting flow regimes ($423 \text{ m}^3 \cdot \text{s}^{-1}$; $2,504 \text{ m}^3 \cdot \text{s}^{-1}$; $10,574 \text{ m}^3 \cdot \text{s}^{-1}$) and are representative of the range of the observed WSE variability for these reaches of the Xingu River, that is,

- low to medium flow ($400\text{--}740 \text{ m}^3 \cdot \text{s}^{-1}$) with a strong downstream control because of VS#5 and VS#3,

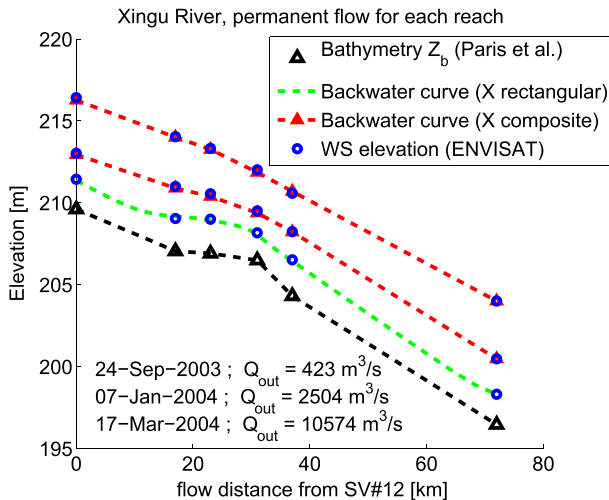


FIGURE 6 Flow lines simulated with backwater curve equation (cf., Section 3.2) compared with ENVISAT measurements at five virtual gauging stations

- intermediate flow ($740\text{--}2,020 \text{ m}^3 \cdot \text{s}^{-1}$) with a moderate downstream control because of VS#5 and VS#3, and
- high flow ($>2,020 \text{ m}^3 \cdot \text{s}^{-1}$) with apparently no downstream control because of VS#5 and VS#3.

As shown in Figure 6, the model's behavior follows observations, and the variability of the river morphology is more filtered by the water surface for higher flow conditions, which indicates less downstream control, especially for the upstream VS#5 and VS#3. The hydraulic significance of the bathymetry profile $Z_0(x)$ from Paris et al. (2016) for this ungauged study zone is therefore corroborated by the hydrodynamic signature of the flow determined by satellite altimetry.

Simulated rating curves are represented along with the "altimetric rating curves" used as boundary conditions for simulating the flow lines (Figure 7). The values are consistent with differences smaller than the uncertainties from the altimetric measurements of the WSE. Hence, a power law stage-discharge relationship can be reproduced with the effective geometry-friction parameterization. The relative errors of the WSE are explained by the histogram on the right panel of Figure 7, which shows the differences between simulated and observed WSE in meters. The differences in the WSE simulated over the 8-year period rarely exceeded $\pm 30 \text{ cm}$ and are mostly between $\pm 10 \text{ cm}$, that is a few percent of relative error on water depth, and on the order of the accuracy of the ENVISAT measurements according to Santos da Silva et al. (2012) and Santos da Silva et al. (2010). Thus, our simple modeling hypothesis (discussed in Section 5.2) and calibration procedure are sufficient for reproducing a large range of flow regimes on a braided river with a state-of-the-art remotely sensed dataset.

5 | DISCUSSION

In this section, we first discuss the impact of the WS measurement accuracy and the related hydraulic visibility as defined above. Then we investigate the impact in terms of simulated water levels of modeling hypothesis on the cross section shape and roughness variability. Following the method used to build the effective hydraulic model proposed in Section 3 and starting from highly simplified cross section shapes and roughness parameterizations, several configurations have been tested, and their limitations are highlighted here. Then, physical interpretations of the flow simulated with the effective model and a calibrated

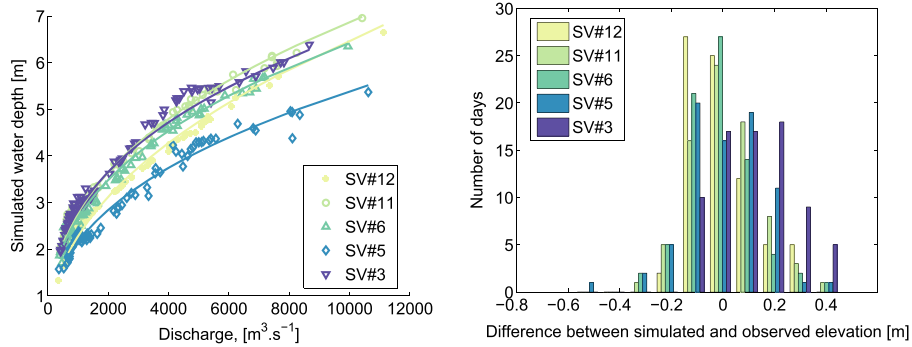


FIGURE 7 (Left) Simulated versus reference rating curves (continuous lines) from Paris et al. (2016). (Right) Histogram of the water surface elevation difference between ENVISAT measurements and simulations

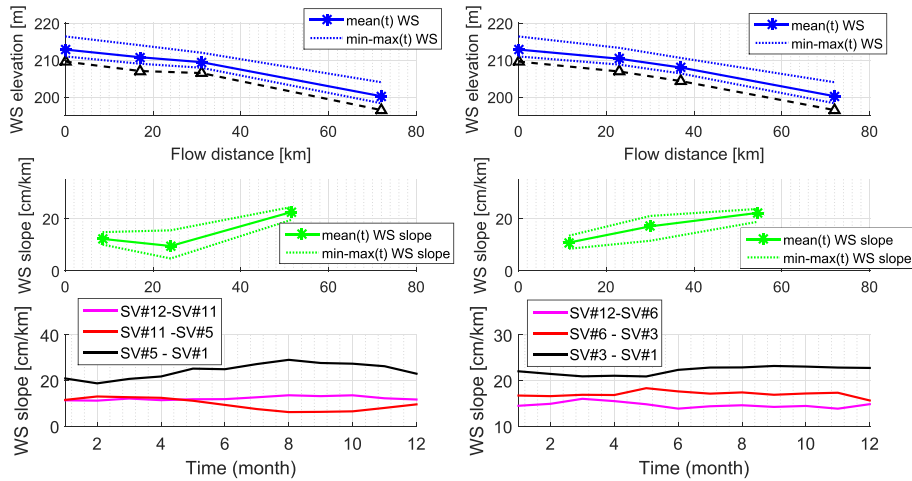


FIGURE 8 Sensitivity analysis of hydraulic visibility with respect to the spatial density of the measurement accuracy. Xingu River crossings by ENVISAT at (Left) $VS\# = [12, 11, 5, 1]$, (right) $VS\# = [12, 6, 3, 1]$

parameter set consisting in roughness values varying in space and in function of water depth are presented.

5.1 | Impact of the measurement accuracy on hydraulic visibility

How does the spatial density of WSE measurements may affect hydraulic visibility? A sensitivity analysis of the spatial sampling has been performed, and two situations with lower virtual station densities are reported in Figure 8. In both cases, the observation of the riffle located between VS#11 and VS#5 (cf., Section 4.2) is deteriorated by considering only two virtual stations among four (VS# 11 and 5; VS# 6 and 3). In both cases, the water surface slope signal is more flat, and the highest WS slope value is approximately 22 cm/km in August for the last reach (VS# 5-1 or VS# 3-1), whereas the value was originally 35 cm/km for reach VS#5-3. This finding highlights the importance of depicting certain details, such as a reach with a length of 6 km at a precise location for our study area, to distinguish different flow regimes. The location and appropriate reach length may depend on the geomorphological configuration and hydrological region.

How will slope uncertainty from SWOT data impact hydraulic visibility? From the SWOT science requirement document (Rodriguez, 2012), the expected slope accuracy after processing elevations over a maxi-

imum of 10 km of flow distance should be 1.7 cm/km or better for river widths greater than 100 m. For the studied reach of the Xingu River, this error on water surface slope represents 34% of the lowest water surface slopes (pool) and 4% of the highest slope values calculated from ENVISAT data. Different reach behaviors can still be distinguished. Slope errors may have a greater impact on studies of river reaches with low slope values such as for low land rivers or for pools. For a given river, the hydraulic visibility may also depend on time periods—even seasons for some hydrological regimes. Indeed, if the slope measurement error is greater than the slope variability for a given time period, there is no hydraulic visibility.

5.2 | Sensitivity analysis to the effective model complexity

A central question in river modeling is the level of complexity required to incorporate potentially nonlinear behaviors across a large range of flow regimes. However, such a model must remain parsimonious (with respect to the number of parameters) to facilitate or allow for its calibration using a dataset of reasonable size.

Several models are tested on the ENVISAT dataset following the cal/val method presented above, and the results are presented for the whole flow lines dataset in Figure 9. An initial simple model consists

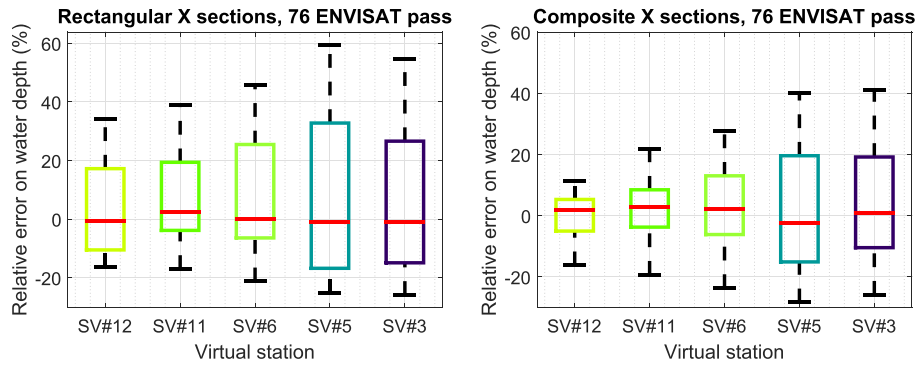


FIGURE 9 Sensitivity analysis with respect to the model hypothesis. Relative error between the modeled WSE and ENVISAT data for simulated water depths over the whole dataset, that is, 76 satellite overpass between 13/11/2002 and 22/09/2010. Test of the modeling hypothesis: (left) rectangular cross section with low-low width (cf., Table 1) and constant calibrated roughness $K_s = [20, 19, 17, 13, 15, 16]$, (right) effective cross sections with constant calibrated roughness [20, 20, 18, 14, 15, 16]

rectangular river cross sections with constant roughness values for all flow regimes, and it is calibrated for each cross section. Under low-flow width conditions, Figure 9 (left) shows that the relative errors of the WSEs are more important and spread with a minimum interquartile range of 20% compared with the less than 10% relative error for the effective cross-section shape and variable calibrated roughness (denoted as \mathcal{M}_{eff}). Moreover, maximal errors on the order of 40% of the water depth or more are observed. This model cannot simulate a large range of flow regimes. Comparable model errors are obtained if a high flow width is used, although the calibrated roughness values are slightly smaller—results are not presented here. These results demonstrate the coupled influence of roughness and cross-sectional geometry.

Because low-flow and high-flow top widths are available, they are both used to set effective cross section shapes (cf., Figure 3) openings for high water levels. Again as shown in Figure 9 (right), a constant roughness coefficient for each effective cross section does not allow for the correct reproduction of all flow regimes. This finding is particularly true for the last three sections, which have interquartile ranges of approximately 20%, 35%, and 30% compared with a less than 10% relative error with \mathcal{M}_{eff} . For all of the VS, the interdecile range has a greater than 20% relative error and a greater than 50% relative error for the last three sections, whereas the VS have a relative error on the order of or lower than 20% relative error with \mathcal{M}_{eff} . Thus, the flow behavior appears to be more nonlinear across the range of tested flow regimes for the last three sections.

Globally, for constant roughness values over time, the results with a rectangular cross section are worse than those with an effective cross section, which promotes the use of a low-flow and a high-flow width. Moreover, in both cases, a constant roughness over time appears to be an insufficient modeling hypothesis and cannot account for the nonlinear behavior of the observed flow on real complex geometries. The results provided in Section 4.4 show the benefit of using roughness that varies in time because relative errors are relatively small. Moreover calibrating the 15 roughness values over the entire surface elevation dataset reduces the errors; thus, despite its modest size, the calibration dataset can constrain the model.

5.3 | Interpretation of the effective hydraulic parameters

As previously stated, river flow dynamics are significantly controlled by basal friction and river morphology, or variations in the river bed slope and/or variations in the channel cross-sectional shape. In this study, a multithread river is modeled under the hypothesis of a single channel with an effective roughness coefficient. Indeed, the wetted perimeter of an effective single-thread section may be lower than the total wetted perimeter of all threads, even for the same wetted surface. Lower values of K_s , which indicates higher friction, were determined for VS#5 and VS#3 for low to intermediate flows. Therefore, a higher friction is required to simulate flow lines with our single-thread representation of a braided river reach under low-flow conditions.

For a given spatial scale, a set of effective cross sections, characterized by their roughness K_s and geometry (cross-sectional wetted surface and perimeter), is expected to reproduce a similar flow line. For a specific discharge value, redefining the cross section geometry and roughness produces a velocity (uniform on a cross section by definition of the 1D Saint-Venant equations) that may be different from the observed velocities. The resolution of the observation grid and crossflow and along the flow distance imposes a scale for averaging real physical and hydraulic properties in both directions. Nevertheless, the use of effective roughness—and geometries with a single-thread representation—appears to be feasible for braided rivers. Indeed, for this dataset of 76 ENVISAT overpasses, the flow line elevation is fairly well approximated with an average relative error lower than 2.4% (Figure 6).

6 | CONCLUSIONS AND PERSPECTIVES

We demonstrate that hydraulic information can be retrieved from current altimetric data over a braided reach of a mid-size river. We used six VS located on an ungauged reach of the Xingu River, which is a tributary of the Amazon River. The current accuracy and spatial resolution of the current altimetry data are sufficient to detect a potential slope break of bathymetry for different flow regimes. The spatial variability of this river's morphology is more filtered by higher flow conditions, as predicted by hydrodynamic laws. Moreover, different hydraulic

behaviors have been depicted from the comparative analysis of the WSE and slope variations over time between VS. Downstream control caused by a constriction in the river width and/or slope break and/or real rugosity variations was identified for two reaches.

This study also provides a simple and effective representation of braided river sections/reaches that may be adapted to “state-of-the-art data” from satellite altimetry and imagery. The calibration and validation results of simulated WSEs are consistent with ENVISAT data, and the differences are smaller than measurement uncertainties. Moreover, the hydrodynamical signature of the flow modeled with the effective river representation is consistent with the WSE and slopes derived from satellite altimetry. Interestingly, a roughness coefficient that varies with the water depth and a single channel representation allow for the reproduction of flow lines of braided river reaches of 5 to 35 km in length. The model covers a wide range of flow regimes, including low-flow regimes where higher effective roughness values appeared necessary to account for the higher friction certainly caused by flow partitioning among threads and to high water season where the forest is flooded and most of the threads connected.

Only remotely sensed data and a hydrologic model are required to establish rating curves and produce an effective hydraulic model. Therefore, this method is applicable for ungauged reaches, such as the studied reach on the Xingu River. In addition, this kind of approach for determining a river bathymetry is a necessary first step for assimilating remotely sensed water elevations (or even water extents) into a hydraulic or hydrologic chain.

Moreover, this paper introduces the concept of hydraulic visibility, which describes the potential for observing hydrological responses and hydraulic variabilities, including the hydrodynamic signature of control sections, of a river reach, or network with remote sensing. Water surface slope variability in time and space reveals to be a powerful proxy for characterizing the hydraulic behavior of river reaches. It is of particular interest for the future satellite mission SWOT, which will offer interesting perspectives in terms of hydraulic visibility for studying flow variability at finer spatiotemporal scales as well as physical scales. Further analysis may also exploit the complementarity of in situ measurements such as bathymetry and flow velocity measurements. More detailed characterizations of water surface slopes and their spatiotemporal variabilities would help define river reaches and characterize their hydraulic unicity. Such characterization could be of interest for inverse approaches based on SWOT data and used to infer spatially distributed river discharges. Further investigations, especially with regard to water surface slopes, could also exploit the information derived from combinations of remotely sensed data from different satellite missions to provide hydrological predictions at ungauged locations.

ACKNOWLEDGMENTS

The authors gratefully acknowledge CNES for post-doc grant for the first author and also the TOSCA grant, which benefited all authors.

REFERENCES

Alsdorf, D., Bates, P., Melack, J., Wilson, M., & Dunne, T. (2007a). Spatial and temporal complexity of the Amazon flood measured from space. *Geophysical Research Letters*, 34(8), 1944–8007.

Alsdorf, D. E., & Lettenmaier, D. P. (2003). Tracking fresh water from space. *Science*, 301(5639), 1491–1494. Available from: <http://www.sciencemag.org/content/301/5639/1491.short>

Alsdorf, D. E., Rodríguez, E., & Lettenmaier, D. P. (2007b). Measuring surface water from space. *Reviews of Geophysics*, 45(2), RG2002. doi: 10.1029/2006RG000197

Bates, P. D., Wilson, M. D., Horritt, M. S., Mason, D. C., Holden, N., & Currie, A. (2006). Reach scale floodplain inundation dynamics observed using airborne synthetic aperture radar imagery: Data analysis and modelling. *Journal of Hydrology*, 328(1), 306–318.

Berry, P., Garlick, J., Freeman, J., & Mathers, E. (2005). Global inland water monitoring from multi-mission altimetry. *Geophysical Research Letters*, 32(16) doi: 10.1029/2006RG000197

Biancamaria, S., Andreadis, K. M., Durand, M., Clark, E. A., Rodríguez, E., Mognard, N. M., & Oudin, Y. (2010). Preliminary characterization of SWOT hydrology error budget and global capabilities. *IEEE Journal of Selected Topics in Applied Earth Observations and Remote Sensing*, 3(1), 6–19.

Biancamaria, S., Durand, M., Andreadis, K. M., Bates, P. D., Boone, A., Mognard, N. M., & Clark, E. A. (2011). Assimilation of virtual wide swath altimetry to improve arctic river modeling. *Remote Sensing of Environment*, 115(2), 373–381. Available from: <http://www.sciencedirect.com/science/article/pii/S0034425710002816>

Biancamaria, S., Lettenmaier, D. P., & Pavelsky, T. M. (2016). *Surveys in Geophysics*, 37, 307. doi: 10.1007/s10712-015-9346-y

Birkett, C. M. (1998). Contribution of the TOPEX NASA radar altimeter to the global monitoring of large rivers and wetlands. *Water Resources Research*, 34(5), 1223–1239.

Birkinshaw, S. J., Moore, P., Kilsby, C. G., O'Donnell, G. M., Hardy, A. J., & Berry, P. A. M. (2014). Daily discharge estimation at ungauged river sites using remote sensing. *Hydrological Processes*, 28(3), 1043–1054. doi: 10.1002/hyp.9647

Birkinshaw, S., O'Donnell, G., Moore, P., Kilsby, C., Fowler, H., & Berry, P. (2010). Using satellite altimetry data to augment flow estimation techniques on the Mekong river. *Hydrological Processes*, 24(26), 3811–3825.

Bjerklie, D. M., Moller, D., Smith, L. C., & Dingman, S. L. (2005). Estimating discharge in rivers using remotely sensed hydraulic information. *Journal of Hydrology*, 309(1–4), 191–209. Available from: <http://www.sciencedirect.com/science/article/pii/S0022169404005724>

Calmant, S., & Seyler, F. (2006). Continental surface waters from satellite altimetry. *Comptes Rendus Geoscience*, 338(14–15), 1113–1122. La Terre observée depuis l'espace Observing the Earth from space. Available from: <http://www.sciencedirect.com/science/article/pii/S1631071306001210>

Calmant, S., Seyler, F., & Cretaux, J. (2008). Monitoring continental surface waters by satellite altimetry. *Surveys in Geophysics*, 29(4–5), 247–269.

Chen, J. L., Wilson, C. R., & Tapley, B. D. (2010). The 2009 exceptional Amazon flood and interannual terrestrial water storage change observed by GRACE. *Water Resources Research*, 46(12). doi: 10.1029/2010WR009383

Chow, V. T. (1959). *Open-channel hydraulics*. New-York, USA: Mc Graw-Hill.

Créaux, J., & Birkett, C. (2006). Lake studies from satellite radar altimetry. *Comptes Rendus Geoscience*, 338(14–15), 1098–1112. La Terre observée depuis l'espace Observing the Earth from space. Available from: <http://www.sciencedirect.com/science/article/pii/S1631071306002318>

Durand, M., Gleason, C. J., Garambois, P. A., Bjerklie, D. M., Smith, L. C., Roux, H., & Schubert, J. Moderate revisions. An intercomparison of remote sensing river discharge estimation algorithms from measurements of river height, width, and slope. *Water Resources Research*.

Durand, M., Neal, J., Rodriguez, E., Andreadis, K. M., Smith, L. C., & Yoon, Y. (2014). Estimating reach-averaged discharge for the River Severn from measurements of river water surface elevation and slope. *Journal of Hydrology*, 511, 92–104. Available from: <http://www.sciencedirect.com/science/article/pii/S002216941400002X>

- Frappart, F., Ramillien, G., & Ronchail, J. (2013a). Changes in terrestrial water storage versus rainfall and discharges in the Amazon basin. *International Journal of Climatology*, 33(14), 3029–3046.
- Frappart, F., Seoane, L., & Ramillien, G. (2013b). Validation of GRACE-derived terrestrial water storage from a regional approach over South America. *Remote Sensing of Environment*, 137(0), 69–83. Available from: <http://www.sciencedirect.com/science/article/pii/S0034425713002010>
- Frappart, F., Calmant, S., Cauhopé, M., Seyler, F., & Cazenave, A. (2006). Preliminary results of {ENVISAT} ra-2-derived water levels validation over the Amazon basin. *Remote Sensing of Environment*, 100(2), 252–264. Available from: <http://www.sciencedirect.com/science/article/pii/S0034425705003585>
- Garambois, P.-A., & Monnier, J. (2015). Inference of effective river properties from remotely sensed observations of water surface. *Advances in Water Resources*, 79, 103–120. doi: 10.1016/j.advwatres.2015.02.007
- Getirana, A., & Peters-Lidard, C. (2012). Water discharge estimates from large radar altimetry datasets in the Amazon basin. *Hydrology and Earth System Sciences Discussions*, 9(6), 7591–7611.
- Gleason, C. J., & Smith, L. C. (2014). Toward global mapping of river discharge using satellite images and at-many-stations hydraulic geometry. *Proceedings of the National Academy of Sciences*, 111(13), 4788–4791. Available from: <http://www.pnas.org/content/111/13/4788.abstract>
- Gleason, C. J., Smith, L. C., & Lee, J. (2014). Retrieval of river discharge solely from satellite imagery and at-many-stations hydraulic geometry: Sensitivity to river form and optimization parameters. *Water Resources Research*, 50(12), 9604–9619. doi: 10.1002/2014WR016109
- Hess, L. L., Melack, J. M., Novo, E. M., Barbosa, C. C., & Gastil, M. (2003). Dual-season mapping of wetland inundation and vegetation for the central Amazon basin. *Remote Sensing of Environment*, 87(4), 404–428. Available from: <http://www.sciencedirect.com/science/article/pii/S0034425703002025>
- Hess, L. L., Melack, J. M., Filoso, S., & Wang, Y. (1995). Delineation of inundated area and vegetation along the amazon floodplain with the SIR-C synthetic aperture radar. *Geoscience and Remote Sensing, IEEE Transactions on*, 33(4), 896–904.
- Hostache, R., Lai, X., Monnier, J., & Puech, C. (2010). Assimilation of spatially distributed water levels into a shallow-water flood model. part II: Use of a remote sensing image of Mosel River. *Journal of Hydrology*, 390(3-4), 257–268. Available from: <http://www.sciencedirect.com/science/article/pii/S0022169410004166>
- Kim, J. W., Lu, Z., Lee, H., Shum, C., Swarzenski, C. M., Doyle, T. W., & Baek, S. H. (2009). Integrated analysis of piasar/radarsat-1 insar and envisat altimeter data for mapping of absolute water level changes in Louisiana wetlands. *Remote Sensing of Environment*, 113(11), 2356–2365.
- Koblinsky, C. J., Clarke, R. T., Brenne, A. C., & Frey, H. (1993). Measurement of river level variations with satellite altimetry. *Water Resources Research* 29, 6, 1839–1848.
- Koponen, S., Kallio, K., Pulliainen, J., Vepsäläinen, J., Pyhälähti, T., & Hallikainen, M. (2004). Water quality classification of lakes using 250-m modis data. *IEEE Geoscience and Remote Sensing Letters*, 1(4), 287–291.
- Kouraev, A. V., Zakharova, E. A., Samain, O., Mognard, N. M., & Cazenave, A. (2004). Ob' river discharge from topex/poseidon satellite altimetry (1992?2002). *Remote Sensing of Environment*, 93(1-2), 238–245. Available from: <http://www.sciencedirect.com/science/article/pii/S0034425704002184>
- Lee, H., Beighley, R. E., Alsdorf, D., Jung, H. C., Shum, C., Duan, J., & Andreadis, K. (2011). Characterization of terrestrial water dynamics in the congo basin using {GRACE} and satellite radar altimetry. *Remote Sensing of Environment*, 115(12), 3530–3538. Available from: <http://www.sciencedirect.com/science/article/pii/S0034425711003178>
- Leon, J., Calmant, S., Seyler, F., Bonnet, M. P., Cauhopé, M., Frappart, F., & Fraizy, P. (2006). Rating curves and estimation of average water depth at the upper Negro River based on satellite altimeter data and modeled discharges. *Journal of Hydrology*, 328(3–4), 481–496. The {ICWRER} - Symposium in Dresden, Germany. Available from: <http://www.sciencedirect.com/science/article/pii/S0022169406000163>
- Lettenmaier, D. P., & Famiglietti, J. S. (2006). Hydrology: Water from on high. *Nature*, 444(7119), 562–563.
- Maheu, C., Cazenave, A., & Mechoso, C. R. (2003). Water level fluctuations in the Plata basin (South America) from topex/poseidon satellite altimetry. *Geophysical Research Letters*, 30(3), 1143. doi: 10.1029/2002GL016033
- Martinez, J. M., Guyot, J. L., Filizola, N., & Sondag, F. (2009). Increase in suspended sediment discharge of the amazon river assessed by monitoring network and satellite data. *Catena*, 79(3), 257–264.
- Meijerink, A. (1996). Remote sensing applications to hydrology: Groundwater. *Hydrological Sciences Journal*, 41(4), 549–561.
- Mercier, F., Cazenave, A., & Maheu, C. (2002). Interannual lake level fluctuations (1993-1999) in Africa from topex/poseidon: Connections with ocean-atmosphere interactions over the Indian Ocean. *Global and Planetary Change*, 32(2-3), 141–163. Available from: <http://www.sciencedirect.com/science/article/pii/S0921818101001394>
- Morris, C. S., & Gill, S. K. (1994). Variation of Great Lakes water levels derived from Geosat altimetry. *Water Resources Research*, 30(4), 1009–1017.
- O'Loughlin, F., Trigg, M. A., Schumann, G. J. P., & Bates, P. D. (2013). Hydraulic characterization of the middle reach of the Congo River. *Water Resources Research*, 49(8), 5059–5070. doi: 10.1002/wrcr.20398
- Paiva, R. C. D., Buarque, D. C., Collischonn, W., Bonnet, M. P., Frappart, F., Calmant, S., & Bulhoes Mendes, C. A. (2013). Large-scale hydrologic and hydrodynamic modeling of the amazon river basin. *Water Resources Research*, 49(3), 1226–1243. doi: 10.1002/wrcr.20067
- Pandey, R. K., Crétaux, J. F., Bergé-Nguyen, M., Tiwari, V. M., Drolon, V., Papa, F., & Calmant, S. (2014). Water level estimation by remote sensing for the 2008 flooding of the Kosi River. *International Journal of Remote Sensing*, 35(2), 424–440.
- Papa, F., Prigent, C., Aires, F., Jimenez, C., Rossow, W., & Matthews, E. (2010). Interannual variability of surface water extent at the global scale. *Journal of Geophysical Research: Atmospheres (1984–2012)*, 115(D12), 1993–2004.
- Papa, F., Prigent, C., & Rossow, W. (2008). Monitoring flood and discharge variations in the large Siberian rivers from a multi-satellite technique. *Surveys in Geophysics*, 29(4-5), 297–317.
- Paris, A., Dias de Paiva, R., Santos da Silva, J., Medeiros Moreira, D., Calmant, S., Garambois, P.-A., Collischonn, W., Bonnet, M.-P., & Seyler, F. (2016). Stage-discharge rating curves based on satellite altimetry and modeled discharge in the Amazon basin. *Water Resources Research*, 52(5), 3787–3814.
- Pellarin, T., Delrieu, G., Saulnier, G. M., Andrieu, H., Vignal, B., & Creutin, J. D. (2002). Hydrologic visibility of weather radar systems operating in mountainous regions: Case study for the Ardeèche catchment (France). *Journal of Hydrometeorology*, 3, 539–555.
- Pfeffer, J., Seyler, F., Bonnet, M. P., Calmant, S., Frappart, F., Papa, F., ... Silva, J. S. D. (2014). Low-water maps of the groundwater table in the central Amazon by satellite altimetry. *Geophysical Research Letters*, 41(6), 1981–1987.
- Prigent, C., Papa, F., Aires, F., Jimenez, C., Rossow, W. B., & Matthews, E. (2012). Changes in land surface water dynamics since the 1990s and relation to population pressure. *Geophysical Research Letters*, 39(8), n/a–n/a. doi: 10.1029/2012GL051276
- Ramillien, G., Cazenave, A., & Brunau, O. (2004). Global time variations of hydrological signals from grace satellite gravimetry. *Geophysical Journal International*, 158(3), 813–826.
- Ramillien, G., Famiglietti, J. S., & Wahr, J. (2008). Detection of continental hydrology and glaciology signals from GRACE: A review. *Surveys in Geophysics*, 29(4-5), 361–374.
- Ramillien, G., Frappart, F., & Seoane, L. (2014). Application of the regional water mass variations from grace satellite gravimetry to large-scale water management in africa. *Remote Sensing*, 6(8), 7379–7405.
- Richey, J. E., Mertes, L. A. K., Dunne, T., Victoria, R. L., Forsberg, B. R., Tancredi, A. C. N. S., & Oliveira, E. (1989). Sources and routing of the Amazon river flood wave. *Global Biogeochemical Cycles*, 3(3), 191–204.
- Rodriguez, E. (2012). SWOT science requirements document. JPL document, JPL.

- Roux, E., Cauhope, M., Bonnet, M. P., Calmant, S., Vauchel, P., & Seyler, F. (2008). Daily water stage estimated from satellite altimetric data for large river basin monitoring/estimation de hauteurs d'eau journalières a partir de données d'altimétrie radar pour la surveillance des grands bassins fluviaux. *Hydrological Sciences Journal*, 53(1), 81–99.
- Roux, E., Santos da Silva, J., Cesar Vieira Getirana, A., Bonnet, M. P., Calmant, S., Martinez, J. M., & Seyler, F. (2010). Producing time series of river water height by means of satellite radar altimetry—a comparative study. *Hydrological Sciences Journal—Journal des Sciences Hydrologiques*, 55(1), 104–120.
- Santos da Silva, J., Calmant, S., Seyler, F., Corrêa Rotunno Filho, O., Cochonneau, G., & Mansur, W. J. (2010). Water levels in the Amazon basin derived from the {ERS} 2 and {ENVISAT} radar altimetry missions. *Remote Sensing of Environment*, 114(10), 2160–2181. Available from: <http://www.sciencedirect.com/science/article/pii/S0034425710001331>
- Santos da Silva, J., Seyler, F., Calmant, S., Rotuno Filho, C., Roux, E., Magalhaes, A., Guyot, J. L., & et al. (2012). Water level dynamics of Amazon wetlands at the watershed scale by satellite altimetry. *International Journal of Remote Sensing*, 33(11), 200–206.
- Schumann, G., Matgen, P., Hoffmann, L., Hostache, R., Pappenberger, F., & Pfister, L. (2007). Deriving distributed roughness values from satellite radar data for flood inundation modelling. *Journal of Hydrology*, 344(1-2), 96–111. Available from: <http://www.sciencedirect.com/science/article/B6V6C-4P4FVB6-6/2/ab1bb3892de9bf18e5ff923cd31f8de6>
- Siddique-E-Akbor, A., Hossain, F., Lee, H., & Shum, C. (2011). Inter-comparison study of water level estimates derived from hydrodynamical model and satellite altimetry for a complex deltaic environment. *Remote Sensing of Environment*, 115(6), 1522–1531. Available from: <http://www.sciencedirect.com/science/article/pii/S00hydrodynamical>.
- Smith, L. C. (1997). Satellite remote sensing of river inundation area, stage, and discharge: A review. *Hydrological Processes*, 11, 1427–1439.
- Smith, L. C., Isacks, B. L., Bloom, A. L., & Murray, A. B. (1996). Estimation of discharge from three braided rivers using synthetic aperture radar satellite imagery: Potential application to ungauged basins. *Water Resources Research*, 32, 2021–2034. 7.
- Smith, L. C., Pavelsky, T. M., & et al. (2009). Remote sensing of volumetric storage changes in lakes. *Earth Surface Processes and Landforms*, 34(10), 1353.
- Tarpanelli, A., Brocca, L., Lacava, T., Melone, F., Moramarco, T., Faruolo, M., & Tramutoli, V. (2013). Toward the estimation of river discharge variations using {MODIS} data in ungauged basins. *Remote Sensing of Environment*, 136(0), 47–55. Available from: <http://www.sciencedirect.com/science/article/pii/S0034425713001375>
- Vörösmarty, C. J., McIntyre, P., Gessner, M. O., Dudgeon, D., Prusevich, A., Green, P., & Liermann, C. R. (2010). Global threats to human water security and river biodiversity. *Nature*, 467(7315), 555–561.
- Vrugt, J. A., Gupta, H. V., Bastidas, L. A., Bouten, W., & Sorooshian, S. (2003). Effective and efficient algorithm for multiobjective optimization of hydrologic models. *Water Resources Research*, 39(8), 1214. doi: 10.1029/2002WR001746
- Xavier, L., Becker, M., Cazenave, A., Longuevergne, L., Llovel, W., & Rotunno Filho, O. C. (2010). Interannual variability in water storage over 2003–2008 in the Amazon basin from GRACE space gravimetry, in situ river level and precipitation data. *Remote Sensing of Environment*, 114(8), 1629–1637.
- Yoon, Y., Garambois, P. A., Paiva, R. C. D., Durand, M., Roux, H., & Beighley, E. (2016). Improved error estimates of a discharge algorithm for remotely sensed river measurements: Test cases on Sacramento and Garonne Rivers. *Water Resources Research*, 52(1), 278–294.
- Zakharova, E. A., Kouraev, A. V., Cazenave, A., & Seyler, F. (2006). Amazon river discharge estimated from topex/poseidon altimetry. *Comptes Rendus Geoscience*, 338(3), 188–196. Available from: <http://www.sciencedirect.com/science/article/pii/S1631071305003226>